# Appearance of colored patterns: pattern–color separability

**Allen B. Poirson* and Brian A. Wandell**

*Department of Psychology, Stanford University, Stanford, California 94305*

Received December 28, 1992; revised manuscript received May 3, 1993; accepted May 11, 1993

We have measured how color appearance of square-wave bars varies with stimulus strength and spatial frequency. Observers adjusted the color of a uniform patch to match the color appearance of the bars in square-wave patterns. We used low-to-moderate square-wave patterns, from 1 to 8 cycles per degree (c/deg). The matches are not photoreceptor matches but rather are established at more central neural sites. The signals at the putative central sites obey several simple regularities. The cone contrast of the uniform patch is proportional to square-wave stimulus strength (color homogeneity) and additive with respect to the superposition of equal-frequency square waves containing different colors (color superposition). We use the asymmetric matches to derive, from first principles, three pattern–color-separable appearance pathways. The matches are explained by two spectrally opponent, spatially low-pass mechanisms and one spectrally positive, spatially band-pass mechanism. The spectral mechanisms that we derive are similar to luminance and opponent mechanisms that are derived with entirely different experimental methods.

## 1. INTRODUCTION

We report the results of experiments designed to measure how color appearance depends on spatial pattern. Subjects set full color matches between a 2-deg box pattern and individual bars in square-wave patterns. The square-wave spatial frequencies ranged from 1 to 8 cycles per degree (c/deg). We used square-wave patterns with a wide range of stimulus strengths and colors.

Two qualitative observations stand out. First, spatial patterns of moderate- and high-spatial-frequency patterns appear mainly light–dark, with little color saturation. This observation plays an important role in the determination of the color bandwidth compression in broadcast television and compression in digital image coding.[1,2] Our data quantify the phenomenon.

Second, the spatially asymmetric color appearance matches are not photopigment matches. For example, moderate-frequency square-wave patterns (4 and 8 c/deg) cannot stimulate the short-wavelength receptors significantly because of axial chromatic aberration. Yet subjects match the bars in these patterns with a stimulus that contains considerable short-wavelength-receptor contrast. The asymmetric color matches are established at neural sites central to the photoreceptors.

The measurements reveal two quantitative properties of the asymmetric matches. First, the cone contrasts of the square wave and of the matching box remain proportional over a large range of stimulus strength. Second, the asymmetric color matches satisfy the principle of superposition with respect to color mixtures of the square waves. When the bar of a square wave of color $\mathbf{s}_1$ matches the box $\mathbf{m}_1$ and a bar of a square wave of color $\mathbf{s}_2$ matches a box $\mathbf{m}_2$, then the bar of a square wave of color $\mathbf{s}_1 + \mathbf{s}_2$ matches the box $\mathbf{m}_1 + \mathbf{m}_2$. Since our data are not photoreceptor matches, this linearity must reflect a linear representation at central neural sites.

Finally, we analyzed the data by using a pattern–color-separable model. Suppose that the input pattern is represented as a neural image on three different pathways, and further suppose that the color appearance of the uniform box and the square-wave bar match when the corresponding locations in the neural images match. Our data are consistent with the hypothesis that neural-image values are equal to the product of three terms: the pathway's sensitivity to the spatial pattern, the pathway's sensitivity to the square wave's color, and the stimulus strength.

We estimated the spatial and spectral tuning of the three pathways both with respect to the image at the cornea and with respect to an estimate of the image at the retina. The color-sensitivity estimates remain unchanged whether we use the corneal or the retinal calculations. In both cases we infer one broadband and two opponent-color pathways. The pattern-sensitivity estimates at the cornea and at the retina differ greatly, suggesting that much of the loss of spatial contrast sensitivity is due to axial chromatic aberration.

Our results arrive at a time when the conflicting results in qualitative analyses of color-mechanism properties that use adaptation have led some authors to suggest the existence of a wide multiplicity of cortical color mechanisms.[3,4] To explain our asymmetric color-matching results, however, we do not need to go beyond a parsimonious three-pathway model.

## 2. METHODS

### A. Experimental Task

Two women with normal color vision (Ishihara plates[5]) and corrected spatial vision (6/6) served as subjects in our experiment. The subjects viewed the screen from 1.82 m.

Throughout the experiment the monitor displayed a neutral, 5-deg uniform background. The test patterns were horizontal square-wave patterns, subtending 2 deg, superimposed upon the uniform background. Subjects

0740-3232/93/122458-13$06.00 © 1993 Optical Society of America

compared the color appearance of one of the bars in the test pattern and a uniform 2-deg-square matching box. Subjects initiated serial presentation of the stimuli, which always consisted of the test pattern, a half-second pause, and then the matching box. Stimulus signals were increased and decreased smoothly with a Gaussian temporal envelope ($\sigma = 140$ m, duration $= \pm 3.5\sigma$). Subjects reviewed the stimulus patterns and continued to adjust the matching box until they were satisfied that they had obtained a complete perceptual match.

During the 8 months of the experiment, each subject made more than 720 match settings. They set at least two matches to the two bars in square-wave patterns of nine different colors, four stimulus-strength levels, and four different spatial patterns. Subjects also set control matches between uniform boxes for all nine color pairs and strength levels ($2 \times 2 \times 9 \times 4 \times 5$). The test patterns included color signals that appeared white–black, red–green, greenish–purple, yellow–blue, and orange–light blue when presented in a uniform field.

### B. Stimulus Representation

For many of our calculations we represent the square-wave colors in a color space defined by the Smith–Pokorny[6,7] cone fundamentals, *LMS*. We use a version of the cone fundamentals in which each spectral responsivity is normalized to a peak value of 1.0. The uniform-background *LMS* coordinates are (7.67, 7.20, 6.31). These three values are proportional to the rate of the photopigment absorptions created by a uniform field in the three cone classes for a standard observer.[8]

We represent the matching box and square waves as three-dimensional vectors. Each entry in the vector specifies the percent modulation of a cone type with respect to the uniform background, $\mathbf{s} = (\Delta L/L, \Delta M/M, \Delta S/S)$. This is the color representation in cone-contrast space. In Table 1 we list the color representation of the square-wave gratings in cone-contrast space, and we describe the color appearance of a uniform box with the same color representation.

It is convenient to define two additional terms to represent the stimulus. First, we define the square-wave stimulus strength to be the vector length of the square-wave color representation in cone-contrast space:

$$\|\mathbf{s}\| = [(\Delta L/L)^2 + (\Delta M/M)^2 + (\Delta S/S)^2]^{1/2}. \quad (1)$$

Second, we define the color direction of a square wave to be the corresponding unit length vector in cone-contrast space, $\mathbf{s}/\|\mathbf{s}\|$. Specifying the square-wave color direction and stimulus strength is equivalent to specifying the square-wave cone-contrast values, since

$$\mathbf{s} = \|\mathbf{s}\| \frac{\mathbf{s}}{\|\mathbf{s}\|}.$$

### C. Monitor Calibration

We presented our stimuli on a 60-Hz noninterlaced color monitor (Hitachi Model 4319) controlled by a graphics card (TrueVision Model ATVista) in an IBM PC-AT. We tested for monitor phosphor additivity and corrected for the nonlinear relationship between graphics card input and monitor output (gamma correction). We measured the spectral power distribution of the monitor's three phosphors weekly, using a spectroradiometer to ensure proper color calibration.[9] We measured the square-wave patterns at several stimulus strengths, using a spatial scanner (Photo Research Model PR-719) to verify the spatial accuracy of the square waves and to verify that gamma correction did not depend on spatial frequency.

### D. Error Measures for Model Evaluations

We report tests of several models of the asymmetric matching data. The models share a common form, $\mathbf{m} = \mathbf{Ts}$, where $\mathbf{s}$ is a vector representing the square-wave cone contrast, $\mathbf{m}$ is a vector representing the observed matching box contrast, and $\mathbf{T}$ is a $3 \times 3$ linear transformation.

For any model transformation $\mathbf{T}$, there will be some difference between the match settings predicted by the model and the subjects' match settings; we require an error measure for choosing a best-fitting transformation. We evaluate the size of the difference between predicted and observed matches relative to our estimate of the match covariance.

Because we have only two replications of each match, we must make some guesses about the appropriate covariance matrix. In this paper we report the results of minimizing with respect to a single covariance matrix, $\mathbf{\Sigma}$. This covariance matrix is derived by combining all the matches in the control condition in which both patterns are a uniform box. We also have evaluated our models by using other error measures. We have performed minimizations with respect to the CIELUV metric space, *LMS* space, and we have used separate covariance matrices derived from matches made to each spatial pattern. The results that we obtain by using all these different error measures lead to the same qualitative conclusions, although specific

**Table 1. Cone Contrast of Square-Wave Color Pairs and Appearance Description**

| $L^a$ | $M^a$ | $S^a$ | Appearance Description[b] |
|---|---|---|---|
| 0.490 | 0.522 | −0.596 | Bright green |
| −0.490 | −0.522 | 0.596 | Purple |
| 0.490 | 0.522 | 0.000 | Light green |
| −0.490 | −0.522 | 0.000 | Bluish purple |
| 0.000 | 0.000 | 0.745 | Light bluish purple |
| 0.000 | 0.000 | −0.745 | Olive green |
| 0.059 | −0.049 | 0.000 | Pinkish red |
| −0.059 | 0.049 | 0.000 | Aqua green |
| 0.059 | −0.049 | −0.596 | Rust orange |
| −0.059 | 0.049 | 0.596 | Aqua blue |
| 0.490 | 0.522 | 0.596 | Greenish white |
| −0.490 | −0.522 | −0.596 | Brownish black |
| 0.549 | 0.473 | −0.596 | Yellow |
| −0.549 | −0.473 | 0.596 | Blue |
| 0.432 | 0.571 | 0.000 | New leaf green |
| −0.432 | −0.571 | 0.000 | Reddish purple |
| 0.600 | 0.590 | 0.476 | White (subject JL only) |
| −0.600 | −0.590 | −0.476 | Dark gray (subject JL only) |
| 0.127 | 0.152 | 0.798 | Purplish blue (subject AW only) |
| −0.127 | −0.152 | −0.798 | Dark olive green (subject AW only) |

[a]Only the highest cone-contrast values are given.
[b]Spatial pattern is a uniform, square, 2-deg field.

parameters do vary. We continue to explore other statistical models of the data set.

The specific error measure that we have minimized is shown in Eq. (2). Denote the difference between the observed and the predicted match as the column vector $\mathbf{e}_i$. We minimize the error measure

$$\sum_{i=1}^{n} (\mathbf{e}_i^t \boldsymbol{\Sigma}^{-1} \mathbf{e}_i)^{1/2}. \tag{2}$$

This error measure is equivalent to transforming the model deviations into a color space in which the difference between the mean match and each individual match in the control condition forms a spherical cloud with unit variance and measuring the Euclidean distance in the new color space.[10,11] We call the new color space the spherical color space. When we report errors in terms of the vector length in this space, we use the term spherical units.

This error measure yields the same minimum for any color space related by a linear transformation. To see this, notice that when the observed matches $\mathbf{m}$ are linearly transformed into a new color space $\mathbf{Lm}$, the errors are also transformed into $\mathbf{Le}_i$. The new covariance matrix becomes $\mathbf{L}\boldsymbol{\Sigma}\mathbf{L}^t$. By substituting these terms into Eq. (2), we see that the error is independent of the color space that we use to represent the data. When the same data are represented in a new color space so that $\mathbf{m}' = \mathbf{Lm}$, $\mathbf{s}' = \mathbf{Ls}$, and $\mathbf{m}' = \mathbf{T}'\mathbf{s}'$, the minimization procedure finds model transformations $\mathbf{T}$ and $\mathbf{T}'$, which are related by $\mathbf{T}' = \mathbf{LTL}^{-1}$.

We used the iterative search procedure STEPIT[12] to perform the error minimizations. We repeated the minimization search procedure starting at several different initial parameter locations to ensure against finding local minima in the error surface.

## 3. EXPERIMENTAL RESULTS

### A. Asymmetric Pattern Matches Are Not Photopigment Matches

Figure 1 illustrates how color saturation decreases as spatial frequency increases and that the asymmetric matches are not photopigment matches. The left-hand panel shows the chromaticity coordinates of the bars in an 8-c/deg square wave. The chromaticity coordinates of the matches to these bars are shown in the right-hand panel. Had the asymmetric color matches been physical matches, the two graphs would have been identical. Instead, the matches set to the moderate-frequency square waves occupy a much smaller portion of the chromaticity diagram, illustrating the reduced saturation in the color appearance of the 8-c/deg pattern.

### B. Precision in the Task

We evaluate our models of these appearance matches by comparing a model's residual error with the precision obtained in our spatially asymmetric color-matching task. We define precision as the difference between the average match in a particular condition and each individual match. We quantify the magnitude of this difference by calculating the length of the difference vector in spherical color space.

Each panel in Fig. 2 shows the cone contrast of the mean match on the vertical axis and the cone contrast of the individual matches on the horizontal axis for one cone type. The center point in each graph represents the gray background. All cone-contrast values are those measured at the monitor. The deviation about the diagonal line is a visual representation of the precision in the task. The distance of the average deviation for this subject is 2.0 spherical units.

### C. Tests of Color Linearity

The asymmetric color matches for a square wave establish a transformation $\mathbf{T}$ between the color representation of the square-wave bars $\mathbf{s}$ and the color representation of the matching box $\mathbf{m}$. We analyze two main properties of the transformation $\mathbf{T}$.

First, we evaluate color homogeneity. Consider an experiment in which we fix the square-wave frequency $f$ and the color direction $c$ and we measure matches to a series of stimulus strengths. We test whether scaling the square-wave strength also scales the matching box strength. If $\mathbf{s}$ matches $\mathbf{m}$, then does $\alpha\mathbf{s}$ match $\alpha\mathbf{m}$?

Second, we evaluate color superposition. Suppose that $\mathbf{s}$ and $\mathbf{s}'$ are square waves at the same spatial frequency. When $\mathbf{s}$ matches $\mathbf{m}$ and $\mathbf{s}'$ matches $\mathbf{m}'$, will the square wave with color superposition of $\mathbf{s}$ and $\mathbf{s}'$ match $\mathbf{m} + \mathbf{m}'$?

If both of these properties are satisfied, then the transformation $\mathbf{T}$ is linear, and we may represent it with a $3 \times 3$ matrix.

*Color Homogeneity*

Figure 3 illustrates one test of color homogeneity. Each panel shows the homogeneity test for a single dimension of the color representation in cone-contrast space. The horizontal axis of each panel is the cone contrast of the square-wave bar, and the vertical axis is the cone contrast of the matching box. Again, both axes refer to quantities

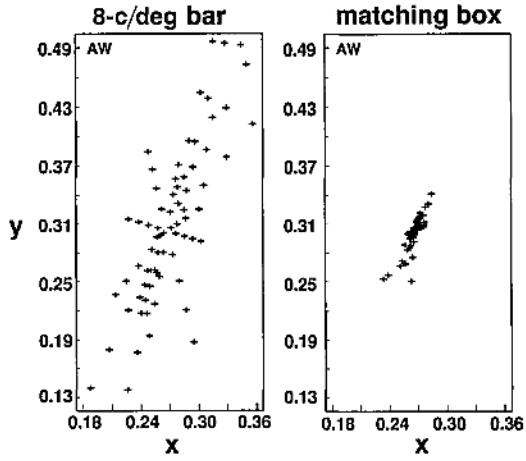


Fig. 1. Chromaticity coordinates $(x, y)$ of the square-wave bars in an 8-c/deg test stimulus (left) and corresponding matching box settings (right). The neutral gray background was $(x, y, Y = 0.27, 0.30, 49.80$ cd/m$^2)$. Were the subject making physical matches, these two graphs would be identical. Instead, the subject's matching box settings occupy a smaller region of the chromaticity diagram, illustrating that the square-wave bars appear desaturated.

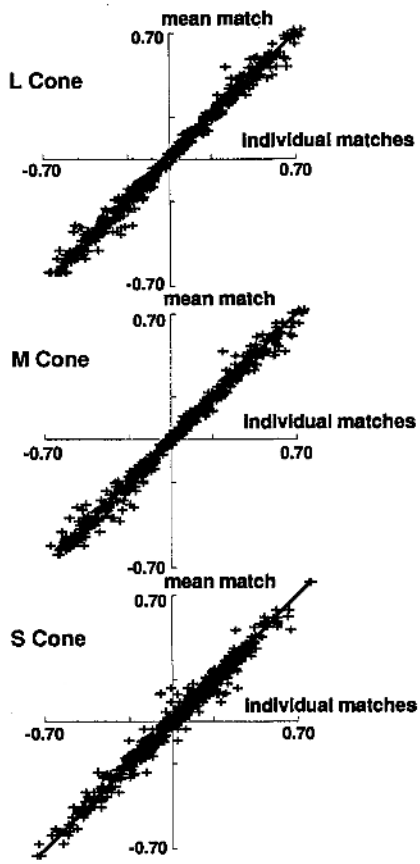


Fig. 2. Visual representation of the precision in the task for subject AW. Cone contrast of mean match on the vertical axis is plotted against the cone contrast of the individual matches on the horizontal axis. The center point represents the background value. Each panel represents a different cone type. The distance of the average deviation is 2.0 spherical units. For our second subject (JL) this value is 1.53.

measured at the monitor, not at the retina. The panel origin represents the mean background.

The square wave used for the data plotted in Fig. 3 was 1 c/deg, and its bars appear orange and light blue. Each data point represents the average of at least two matching box settings. The matches were made at four stimulus-strength levels for each of the two bars, yielding a total of sixteen matches.

Color homogeneity implies that for each test frequency and color-direction condition there is a $3 \times 3$ matrix $\mathbf{T}_{f,c}$ that maps the test stimuli into the matching box settings.[13] This matrix defines a line in three-dimensional space. The lines in the panels represent the best-fitting line through the origin and the data. Color homogeneity holds to the extent that the data fall precisely upon a line. If the subject makes a physical match, the data will fall upon a line with unit slope in each panel. Even at 1 c/deg the matches do not fall upon lines of unit slope.

Each observer collected data for 45 graphs like the one in Fig. 3. Figure 4 contains a subset of these graphs for one square-wave color direction at several spatial frequencies.

In the control condition, when the test pattern is a uniform box (left-hand column), the subject's matching box settings are close to physical matches. As the spatial frequency increases, the slopes tend to decrease, and the matches deviate from physical matches.

The data in Figs. 3 and 4 are typical of the precision of color homogeneity that we have observed. To illustrate the overall quality of the color-homogeneity prediction, we combined the data from all 45 conditions into a single graph. To combine the data, we fitted straight lines through each of the graphs individually; we then merged the data into a single graph that shows the observed and the predicted values. This coarse test of homogeneity is shown for subject AW in the left-hand panel of Fig. 6 below. The average deviation from color homogeneity is 2.79 spherical units.

Color homogeneity serves as a good first-order model of the data. We comment on some of the failures of color homogeneity in more detail at the end of this section.

*Color Superposition*

We test color superposition by comparing matches to the sum of square waves with the sum of matches to square waves. We illustrate the test for one spatial pattern and cone type schematically in Fig. 5. Suppose that a subject's matches to two different square-wave stimuli fall upon the two dotted lines. The additivity prediction is that matches to the sum of the square waves will fall upon the solid line.

Our data set includes measurements in nine color directions for each spatial pattern. The color directions are

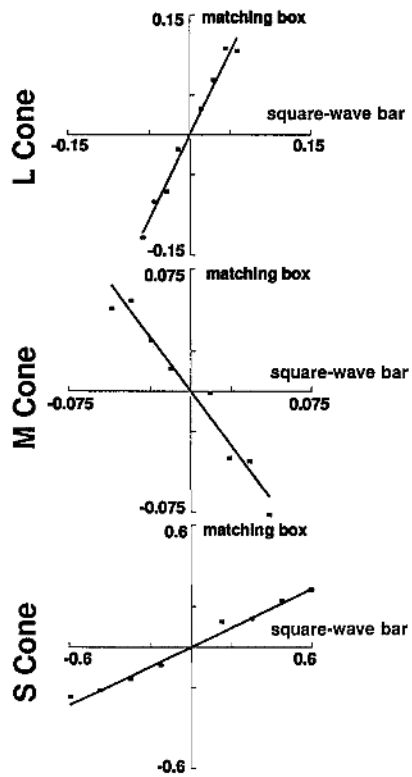


Fig. 3. Definition of subject JL's full-color matches to a 1-c/deg square wave; the square-wave bars appeared orange and light blue. The horizontal axis plots the physical measure of the square-wave bar; the vertical axis plots the subject's matching box setting. The axes are cone contrast, the center represents the background value, and each panel describes the settings for one cone type. The line is the prediction from the best-fitting color-homogeneous model.

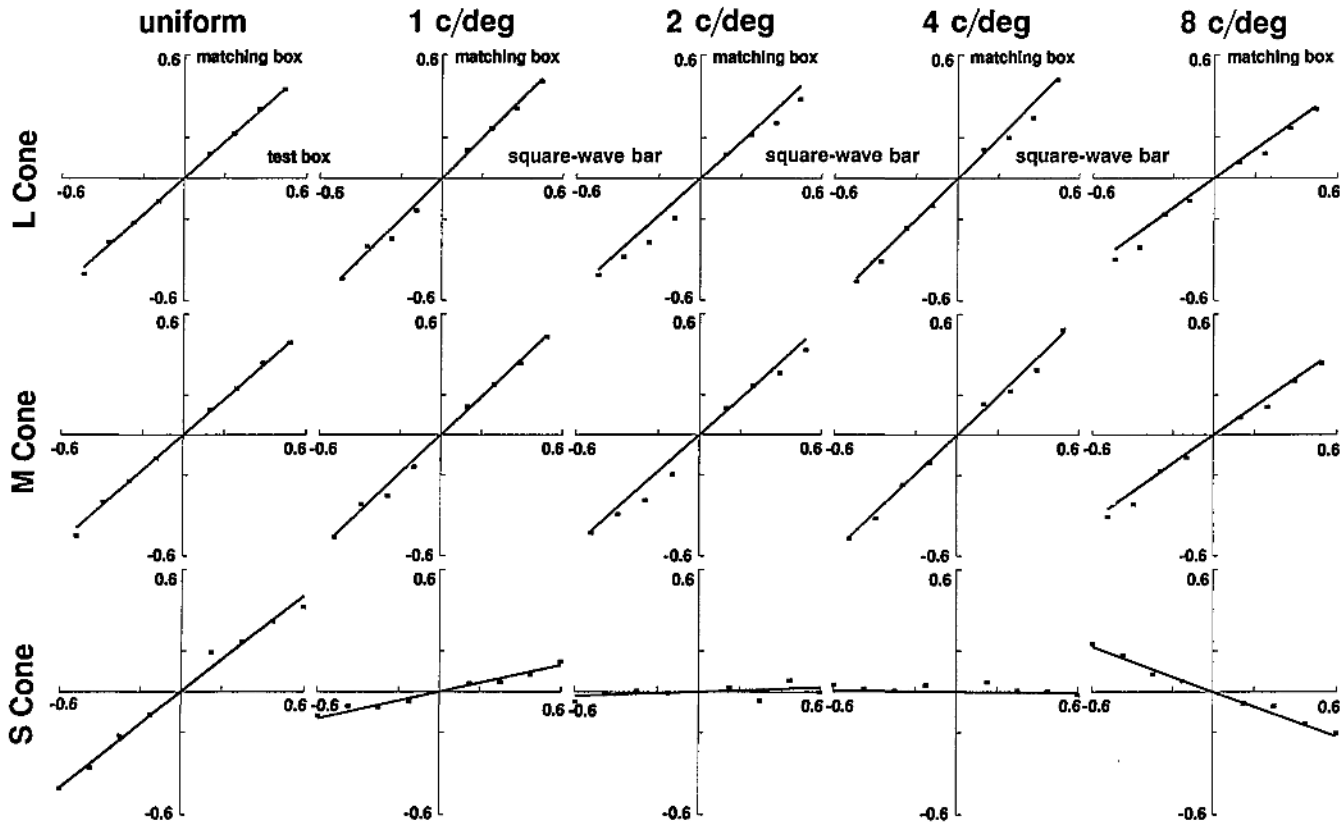


Fig. 4. Each column is as in Fig. 3, for subject JL. The columns show matches for different test frequencies. The square-wave bars were of colors different from those in Fig. 3 and appeared bright green and purple at low spatial frequencies.

interrelated sums. Color superposition implies that there is a single 3 × 3 matrix that maps all test stimuli presented in a given spatial frequency condition into the corresponding matching box setting. We refer to this matrix as $\mathbf{T}_f$, dropping the matrix's dependence on color direction. For each subject and each spatial pattern we solve for the matrix $\mathbf{T}_f$ that minimizes the error described in Section 2 [Eq. (2)].

We plot the observed and the predicted cone contrast, using the color-superposition model for all the asymmetric matches in the middle panel of Fig. 6. Color superposition and color homogeneity are nested hypotheses: in the presence of weak continuity assumptions, superposition implies homogeneity. By comparing the left and the middle graphs of Fig. 6, one can see that the added requirement of color superposition does not worsen the fit substantially.

### D. Pattern–Color-Separable Model

How does the linear transformation $\mathbf{T}_f$ depend on the spatial pattern? We analyze this dependence by casting the asymmetric matching experiment as a neural model. Suppose that three parallel neural pathways code color appearance. The pathways differ in their color and pattern sensitivities. We assume that each pathway forms a neural image of the visual pattern. Two locations in the visual field have the same color appearance when the three pathway values are equal.

We examine the hypothesis that the pathway representations are pattern–color separable. We assume that the value in one neural image is the product of three terms. One term defines the pathway's sensitivity to the square wave's color direction. A second term defines the pathway's sensitivity to the spatial pattern. The third term is the square wave's stimulus strength.

We can express this hypothesis in matrix notation as follows. We represent the terms defining the color-direction sensitivity by the 3 × 3 matrix $\mathbf{C}$. This matrix maps the color-direction vector $\mathbf{s}/\|\mathbf{s}\|$ into the color space defined by the three visual pathways. We represent the sensitivities to the spatial pattern by the 3 × 3 diagonal matrix $\mathbf{D}_f$. Each entry in this matrix scales one pathway's response. We represent the three pathway responses succinctly as

$$\mathbf{D}_f\mathbf{C}\mathbf{s} = \|\mathbf{s}\|\mathbf{D}_f\mathbf{C}\frac{\mathbf{s}}{\|\mathbf{s}\|}.$$

The matrix $\mathbf{C}$ is the same for all different spatial patterns. The diagonal matrix $\mathbf{D}_f$ depends only on the spatial pattern. Because the individual pathways are separable with respect to pattern and color, we call the model pattern–color separable.

Finally, we note that it is possible to follow the pathway responses with an arbitrary nonlinearity without changing any predictions of the model.

### E. Applying the Model to the Experiment

Experimentally, we observe matches between a square-wave bar $\mathbf{s}$ and a box $\mathbf{m}$. By assumption, two stimuli

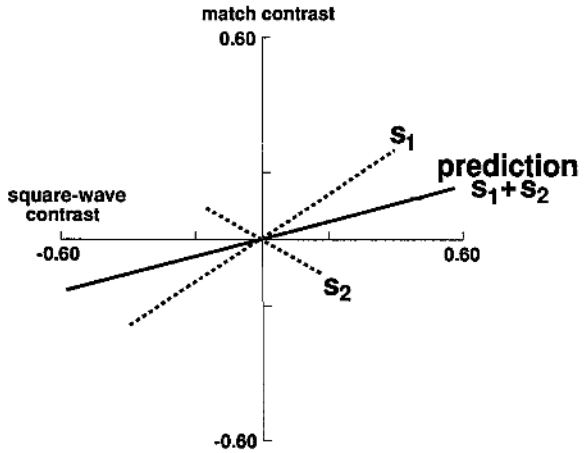


Fig. 5. Additivity predictions for color superposition for one cone type. Suppose that a subject's matches to two different square-wave stimuli fall upon the dotted lines. The additivity prediction is that matches to the sum of the square waves will fall upon the solid line.

match when

$$\mathbf{D}_0\mathbf{C}\mathbf{m} = \mathbf{D}_f\mathbf{C}\mathbf{s}$$

$$\mathbf{m} = \mathbf{C}^{-1}\mathbf{D}_0^{-1}\mathbf{D}_f\mathbf{C}\mathbf{s}. \quad (3)$$

To simplify the notation, and without loss of generality, we assume that $\mathbf{D}_0$ is the identity matrix and are left with

$$\mathbf{m} = \mathbf{C}^{-1}\mathbf{D}_f\mathbf{C}\mathbf{s}. \quad (4)$$

The pattern–color-separable model is restricted compared with the color-homogeneous and color-superposition models. Color homogeneity permits an arbitrary matrix for each color direction and each spatial pattern $\mathbf{T}_{f,c}$. Color superposition permits an arbitrary matrix for each pattern $\mathbf{T}_f$. Pattern–color separability implies that all the matrices $\mathbf{T}_f$ must share a common form, $\mathbf{T}_f = \mathbf{C}^{-1}\mathbf{D}_f\mathbf{C}$, and contain the same color matrix $\mathbf{C}$.

We performed an iterative search to find the collection of similar matrices $\mathbf{T}_f = \mathbf{C}^{-1}\mathbf{D}_f\mathbf{C}$ that minimizes the error measure in Eq. (2). The graph on the right-hand side of Fig. 6 plots the observed and the predicted matches of the pattern–color-separable model. The pattern–color-separability hypothesis does not substantially worsen this visualization of the error. The average length of the residual errors for observers AW and JL is 3.39 and 3.15 spherical units, respectively. The precision of their matches is 2.00 and 1.53 spherical units, respectively.

A second way to quantify the magnitude of the error in the separable model is to calculate the length of the residual vector in CIELUV color space. This space at-

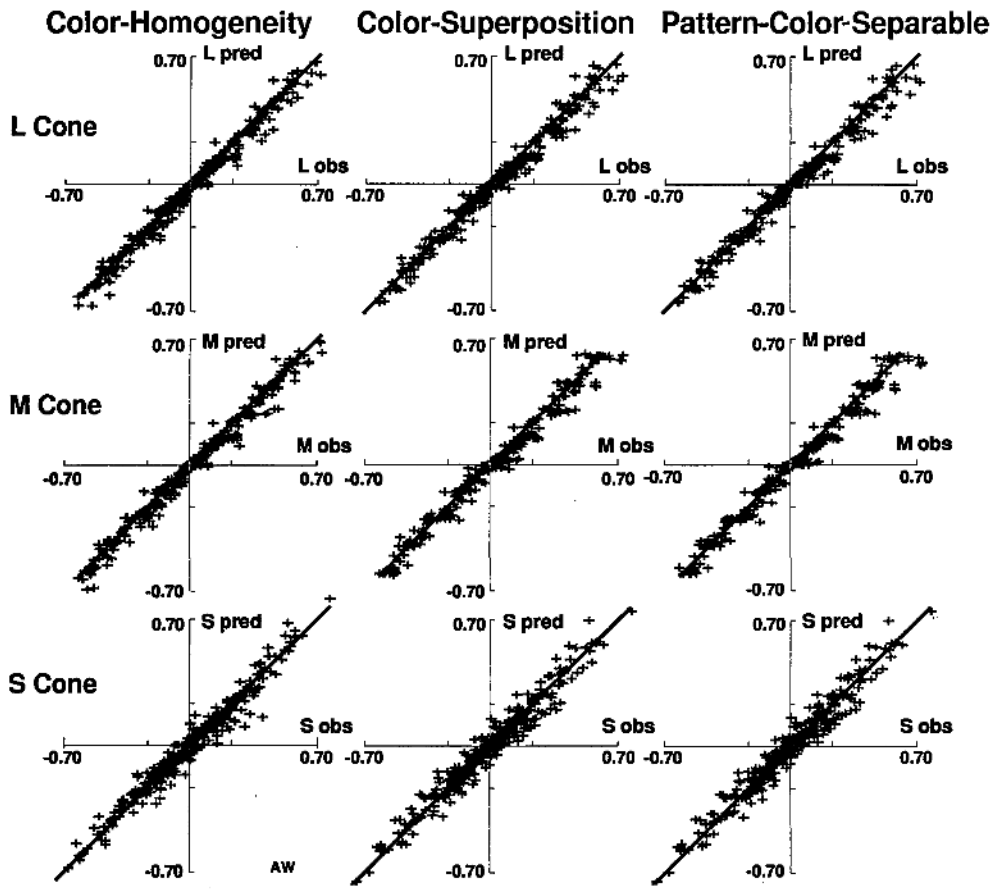


Fig. 6. Each column plots the observed versus predicted matches for subject AW: left-hand column, color-homogeneity model; middle column, color-superposition model; right-hand column, pattern–color-separable model. Each row shows the predictions for a different receptor class. The axes are cone-contrast units measured at the monitor, and the center position represents the background value. The average residual errors for this subject and the three models are 2.79, 3.33, and 3.39 spherical distance units. (For subject JL the values are 2.48, 3.07, and 3.15.) The number of parameters required for fitting the color-homogeneity, color-superposition, and pattern–color-separable models to one subject's data is 135, 45, and 21, respectively.

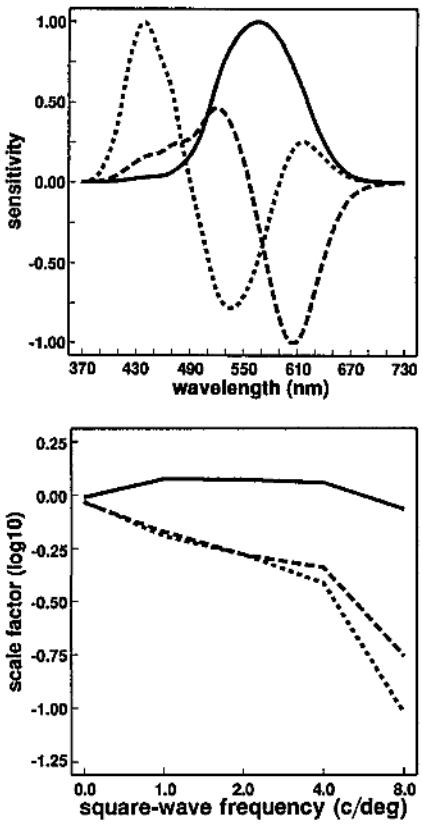


Fig. 7. Pattern–color-separable color (top) and pattern (bottom) functions for subject AW. Spectral and spatial functions from each of the three pathways are drawn with the same type of curve (solid, dashed, or dotted) in both panels.

tempts to make equally discriminable colors equal in length. To calculate this distance measure, $\Delta E_{uv}$, one needs to make an estimate of the observer's white point. We assumed that the uniform background field represented a 20% gray surface. The average length of the residual errors in $\Delta E_{uv}$ units for observers AW and JL is 3.17 and 2.79, respectively. The precision of the matches for AW and JL is 1.87 and 1.47 $\Delta E_{uv}$ units, respectively.

### F. Evaluation of the Model

For many industrial imaging applications, 3–4 $\Delta E_{uv}$ units is considered small, approximately one just-noticeable difference. For some demanding commercial applications involving matches between large areas of paint or fabric placed directly adjacent to one another, $\Delta E_{uv}$ values of 1 or less are required. The difference between the precision of the observers' replications of their matches and the model predictions is ~1 $\Delta E_{uv}$ and also ~1 spherical unit. While pattern–color separability may not be precisely correct, the deviations are small enough that we think it is useful to consider the properties of the mechanisms derived from the observers' matches.

### G. Pattern and Color-Sensitivity-Function Estimates

The pattern–color-separable calculation estimates the color and pattern sensitivities of all three putative pathways. Each row in the matrix **C** defines the spectral responsivity of a pathway that is a weighted sum of the cone photopigment absorptions. The diagonal entries of $\mathbf{D}_f$ define the pattern sensitivity of the pathways. In Appendix A we prove that the matrices $\mathbf{D}_f$ and **C** that we recover from our search are unique up to a scale factor applied to each row of **C**.

For one observer, AW, we plot the spectral responsivity of the three pathways in the top panel of Fig. 7. We plot the pattern sensitivities to the square waves in the bottom panel of Fig. 7. Spectral and spatial functions from one pathway are drawn with the same type of curve in both panels. These pattern-sensitivity plots are not modulation transfer curves, for two reasons. First, our measurements are based on square waves, not sinusoids. Second, and more important, we have not tested pattern superposition. Modulation transfer functions are meaningful only for linear systems.

The formal simplifications from pattern–color separability have a geometric counterpart. First, represent both the matching box settings and the physical signal of the square-wave bars in the color-coordinate frame defined by matrix **C**. Second, scale the axes in this new color space to make the physical signal of the square-wave bars coincident with the matching box settings. The appropriate scale factor for a given axis and spatial pattern $f$ is given in the appropriate entry of the diagonal matrix $\mathbf{D}_f$.

Figure 8 shows subject AW's appearance matches plotted in the pattern–color-separable color-coordinate frame. The lines in each panel are the predictions from the pattern–color-separable fits to her data. The data in each column include the matches from the nine color directions at each spatial frequency. Were the model perfect, all the data would lie upon the solid line drawn in each panel. The slope of the lines at each spatial frequency define a color pathway's pattern sensitivity.

The data from our two subjects are similar. Figure 9 contains the pattern–color-separable mechanisms derived by combining the data from both observers. We tabulate matrix **C** (Table 2) and matrices $\mathbf{D}_f$ (Table 3) for the individual subjects and for the joint fit.

To estimate the precision of our derived functions, we used a resampling procedure.[14] We drew a random sample, with replacement, of 720 color matches from the collection of 720 color matches. For each draw we found the best-fitting pattern–color-separable model and its corresponding spectral and spatial tuning functions. We repeated this process 25 times to obtain 25 estimates of each tuning curve. Figure 9 plots the envelope of the estimates from each draw around the estimate from the true data.

### H. Model Limitations

Separability is an important property; it guides practical measurement and hypothesis formation about the neural representation of visual appearance. We wish to qualify our support, since two assumptions that underlie separability are contradicted in portions of our measurements. We believe that these deviations represent modest but genuine failures of color homogeneity, linearity, or separability.

First, we have observed instances in which the data are not symmetric through the origin. For example, the data from subject AW in the 4-c/deg condition (Fig. 8, fourth column, top panel) are not odd symmetric through the origin. Data in this plot fall primarily above the prediction line. The data appear linear in each quadrant, but the two line segments are themselves not aligned.

Second, we also have observed instances in which the data are not strictly linear. For example, data in the red–green plot in the 1-c/deg condition are more nearly sigmoidal than linear (Fig. 8, second column). The model overestimates the scale factor for small signals in this case. Small decrements fall below the line and small increments fall above the line predicted by the model.

## 4. DISCUSSION

### A. Color Representations

We compare our derived pattern–color-separable representation with four pattern–color-separable representations that extend color representations proposed in other contexts.

Color representation DKL extends the MacLeod–Boynton[15] chromaticity diagram. The representation was first described in a paper evaluating physiological responses in the lateral geniculate nucleus of macaque monkeys[16] (see also Flitcroft[17]). The MJHJ representation was proposed by Müller,[18,19] quantified by Judd,[20] and studied by Hurvich and Jameson[21–23] in unique-hue cancelation experiments. The YIQ representation was defined by the National Television Standards Committee based on a variety of psychophysical measurements involving spatial judgments of color appearance.[24] Guth[25,26] and his colleagues have developed the ATD representation as a coarse summary of a broad variety of different color judgments.

Each color representation defines a color matrix **C**. We extend the color representations to pattern–color representations by searching for diagonal matrices $\mathbf{D}_f$ that minimize Eq. (2) with respect to our data set.

The spectral sensitivities of each color representation are plotted in the top row of Fig. 10. The estimated pattern-sensitivity functions are plotted in the bottom row. Our current error measure does not distinguish strongly between the DKL, MJHJ, and YIQ representations. The difference between these model fits is comparable with the difference that we observe when we apply the best fit from the data of one observer to the data of the other. The ATD representation is somewhat worse. All these color representations, combined with their appropriate spatial functions, fit the pooled data, with $\Delta E_{uv}$ residual errors ranging from 3.61 to 3.89.

### B. Optical Factors

Our analysis has combined the optical and neural components of vision. Can we separate the contributions of these two factors?

Axial chromatic aberration is the most important optical factor limiting the eye's spatial resolution. To estimate the contribution of axial chromatic aberration to the matches, we need an estimate of the optical transfer func-

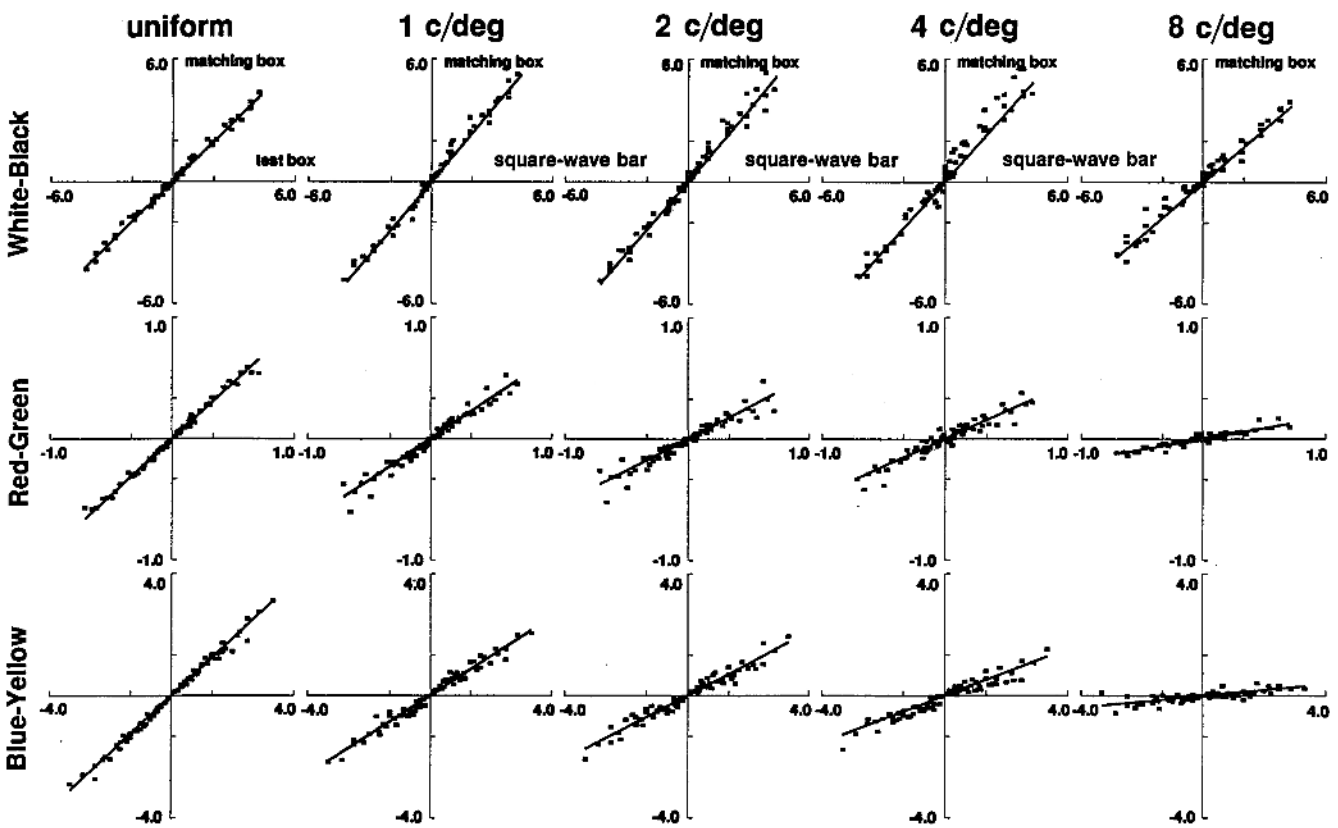


Fig. 8. Subject AW's matches are plotted in the color representation derived from the pattern–color-separable model. Each column contains the data from one spatial pattern, and each row shows the predictions for one of the three color dimensions. The lines are the pattern–color-separable model predictions. Each panel includes matches from all square-wave color pairs.

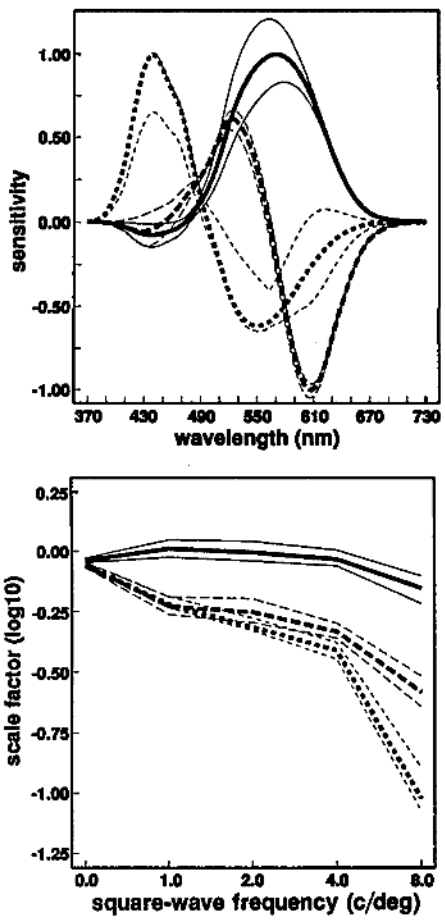


Fig. 9. Pattern–color-separable color (top) and pattern (bottom) functions estimated by combining the data of subjects AW and JL. The envelope (lighter curve) around each bold curve (solid, dashed, or dotted) describes the extreme values from a resampling procedure. See text for details.

tion at different wavelengths. We are unaware of any empirical estimates of this function, so we used an estimate based on a model described by Wandell and Marimont[27] based on methods introduced by Hopkins.[28]

The model assumes that the optics introduce only spherical aberration and that the eye is statically accommodated to 580 nm. In addition, we simplify calculations by treating our square-wave stimuli as sine waves. We use the chromatic aberration data from Wald and Griffin[29] and from Bedford and Wsyzecki[30] to estimate the defocus at each incident wavelength. From photographs we measured our subjects' pupil size diameter under our experimental conditions (5.5 mm). We selected other model eye parameters to match the average human eye.[27]

To discount the effects of axial chromatic aberration, we must estimate the retinal image. We begin with the spectral power distribution of the input signal, which we treat as the sum of monochromatic sinusoids at the same frequency as the square-wave stimulus. The optical transfer function defines the amplitude reduction of each monochromatic sinusoid, yielding the estimated retinal image. We assume that the retinal image is absorbed by the photoreceptors and inert pigments in the usual way, and thus we obtain an estimate of the cone contrasts corrected for axial chromatic aberration.

Figure 11 shows the spectral and spatial tuning functions that arise when we fit the pattern–color-separable model by using our estimate of the cone contrast stimulating the retina. These spectral functions are similar to those shown in Fig. 9; we again find one spectrally broadband function and two spectrally opponent.

After correction for axial chromatic aberration, the pattern-sensitivity functions show only a two-tenths (blue–yellow mechanism) or three-tenths (red–green mechanism) log unit roll-off at our highest frequency. We conclude that the pattern-sensitivity loss that we observe for the whole observer is due mainly to optical factors. Since axial chromatic aberration is due largely to the presence of water in the eye, this factor is likely to be important across species and observers.[17]

### C. Related Literature

*Appearance Measures*

Georgeson and Sullivan[31] asked subjects to match the contrast of sinusoidal patterns at different spatial frequencies and stimulus strengths. The color direction, determined by the oscilloscope phosphor, was the same for both the 5-c/deg standard frequency and the various test frequencies. We test for homogeneity of their data by plotting the contrast of the standard frequency versus the matching contrast of the test frequency in linear coordinates and finding the best-fitting straight line through the origin and data points. We restrict our analysis to stimulus conditions in which the standard grating contrast is 5% or

**Table 2. Color matrices C for the Best-Fitting Pattern–Color-Separable Model[a]**

| Subject | Function | $L$ | $M$ | $S$ | Graph-Curve Type |
|---|---|---|---|---|---|
| JL | W-B | 0.962 | 0.004 | −0.272 | Solid |
| | R-G | −0.658 | 0.751 | −0.049 | Dashed |
| | B-Y | 0.095 | −0.589 | 0.802 | Dotted |
| AW | W-B | 0.999 | 0.009 | 0.000 | Solid |
| | R-G | −0.694 | 0.719 | 0.039 | Dashed |
| | B-Y | 0.397 | −0.751 | 0.528 | Dotted |
| JL and AW | W-B | 0.990 | −0.106 | −0.094 | Solid |
| | R-G | −0.669 | 0.742 | −0.027 | Dashed |
| | B-Y | −0.212 | −0.354 | 0.911 | Dotted |

[a]Each row lists the normalized cone weights used to construct the spectral functions shown in Figs. 7 and 9. The rows are required to be unit length. To create, say, the red-green spectral function for subject AW, plot $(-0.694L + 0.719M + 0.039S)$ as a function of wavelength, where $L$, $M$, and $S$ are the Smith–Pokorny cone fundamentals, each normalized to a peak value of 1.0. W-B, white-black; R-G, red-green; B-Y, blue-yellow.

**Table 3. Values in Matrices $D_f$ for the Best-Fitting Pattern–Color-Separable Model[a]**

| Subject | Frequency | W–B (Solid) | R–G (Dashed) | B–Y (Dotted) |
|---|---|---|---|---|
| JL | Uniform | 0.873 | 0.841 | 0.826 |
| | 1 c/deg | 0.850 | 0.539 | 0.511 |
| | 2 c/deg | 0.797 | 0.542 | 0.413 |
| | 4 c/deg | 0.706 | 0.466 | 0.359 |
| | 8 c/deg | 0.513 | 0.345 | 0.079 |
| AW | Uniform | 0.975 | 0.921 | 0.933 |
| | 1 c/deg | 1.192 | 0.675 | 0.645 |
| | 2 c/deg | 1.180 | 0.527 | 0.527 |
| | 4 c/deg | 1.142 | 0.457 | 0.387 |
| | 8 c/deg | 0.859 | 0.176 | 0.095 |
| JL and AW | Uniform | 0.916 | 0.873 | 0.872 |
| | 1 c/deg | 1.025 | 0.590 | 0.604 |
| | 2 c/deg | 0.987 | 0.559 | 0.485 |
| | 4 c/deg | 0.926 | 0.464 | 0.388 |
| | 8 c/deg | 0.703 | 0.263 | 0.096 |

[a]Each column lists the scale factors for a specified spectral function that are used to construct the spatial scale functions shown in Figs. 7 and 9. W–B, white–black; R–G red–green; B–Y, blue–yellow.

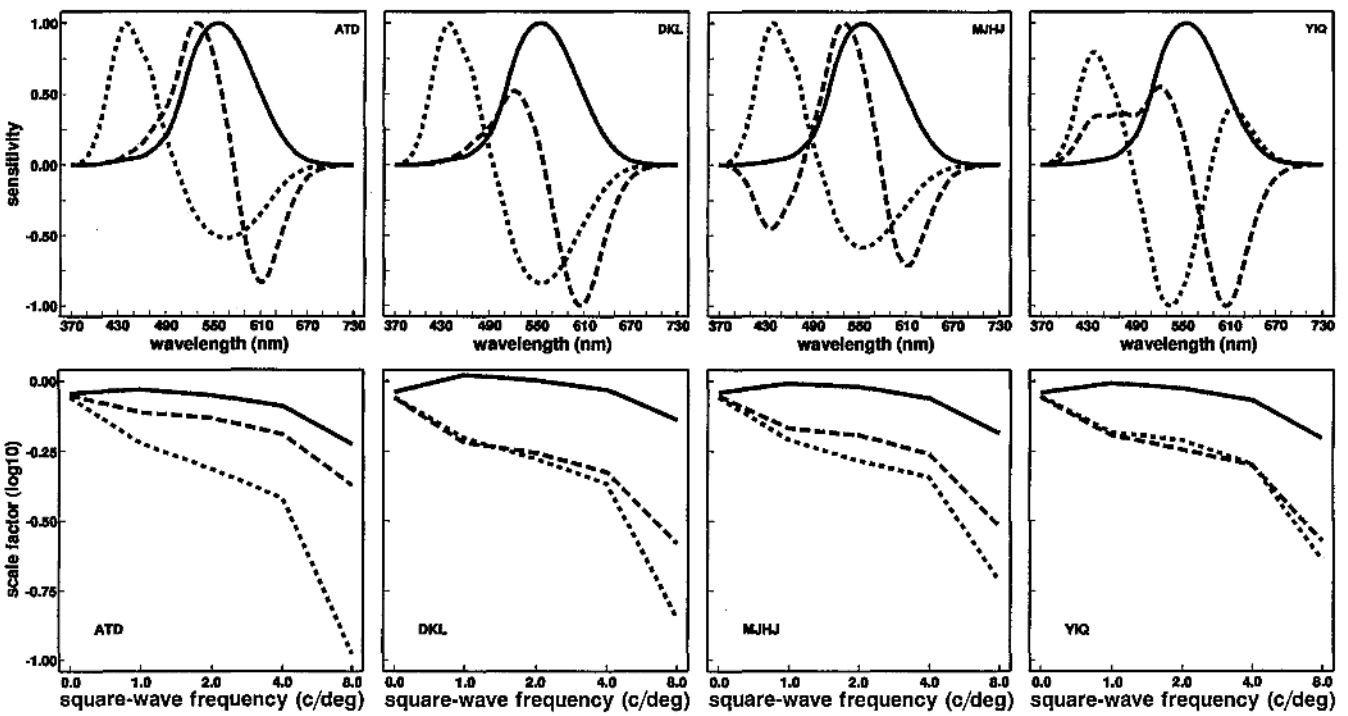


Fig. 10. Color (top) and pattern (bottom) tuning functions for four other color representations. The color sensitivities were taken from the literature, and the pattern sensitivities were determined from a best fit of the pattern–color-separable model. The functions drawn with the same type of curve (solid, dashed, or dotted) belong to common putative pathways.

greater. The test grating spatial frequency is 0.25, 0.5, 1.0, 2.0, 5.0, 10.0, 15.0, 20.0 or 25.0 c/deg.

In Fig. 12 we show the observed versus the predicted contrast settings from the homogeneous models that are best-fitting to the Georgeson–Sullivan data. As in Fig. 6, were the model to fit perfectly, all the points would fall upon the solid diagonal line of slope one. We see that the homogeneous model serves well to predict these contrast match settings. Evidently, the nonlinearities observed by Georgeson and Sullivan are restricted to threshold and near-threshold measurements.

A number of investigators have studied color appearance by using a hue-cancellation paradigm.[32–38] Several of these studies evaluated the linearity of the mechanisms with a variety of techniques. Our experimental paradigm differs greatly from that of hue cancellation in that we require our subjects to make complete appearance matches; thus our results are not directly comparable. Instead, we stress the qualitative similarity between our derived spectral functions and those determined by the hue-cancellation paradigm, which by its nature presupposes opponency.

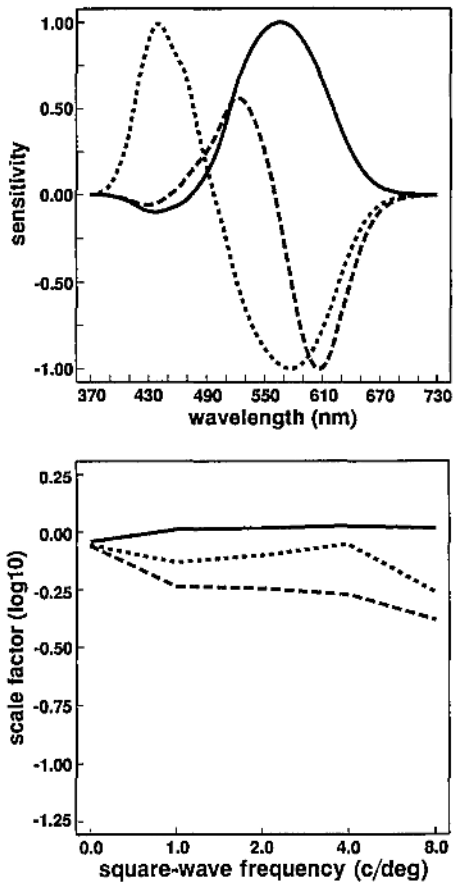


Fig. 11. Pattern–color-separable tuning curves derived from the fit to combined subject data that are corrected for axial chromatic aberration. The curves of the color functions (top) are similar to the curves derived without correction for chromatic aberration (see Fig. 9). The pattern sensitivities (bottom) fall off more slowly with frequency, suggesting that the loss of resolution is due largely to optical factors.

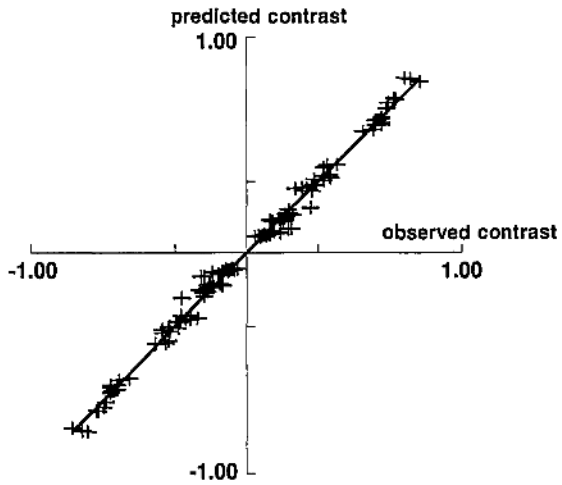


Fig. 12. Observed contrast matches versus contrast matches predicted from homogeneous models fitted to data given by Georgeson and Sullivan.[31] We restrict our analysis to stimulus conditions in which the standard grating contrast is 5% or greater. The test grating spatial frequency is 0.25, 0.5, 1.0, 2.0, 5.0, 10.0, 15.0, 20.0, or 25.0 c/deg. Data points are reflected through the origin. Were the homogeneous model perfect, all the points would fall upon the diagonal line of slope 1.0.

*Threshold Measures*

Much of what we have learned about pattern and color sensitivity comes from threshold experiments.[39–46] Generally, threshold measurements of the pattern sensitivity of putative color pathways begin with two assumptions. First, experimenters often assume that the color sensitivities of the mechanisms are known before the experiment or that these properties can be measured with procedures such as flicker photometry. Second, the experimenter assumes that the pattern and color sensitivities are separable. This assumption is implicit in the act of measurement since, if separability fails, then the pattern and color-sensitivity curves are intertwined and we learn very little from an individual tuning curve.

Our experiments begin with the premise that it is important to test both of these assumptions. The color-appearance experiments that we report here are formulated to test separability and estimate pattern and color tuning. We report elsewhere[47] on similar tests that use threshold data.

## 5. CONCLUSION

When observers match the color appearance of low- and moderate-spatial-frequency square waves with uniform patches, the matching transformation satisfies color homogeneity and color superposition. Examination of the data reveals clearly that these asymmetric color matches are not photoreceptor matches. Rather, the matches depend on an equivalence established at more central sites.

To understand the properties of the signals at these central sites, we analyzed the matching transformation, using a pattern–color-separable model. We used the data to derive, from first principles, the separable pattern and color sensitivities of three central site mechanisms.

## APPENDIX A: UNIQUENESS

The pattern–color-separable model recovers a collection of matrices that determine the spectral and spatial tuning curves of the putative mechanisms. We call these matrices $\mathbf{D}_f$ and $\mathbf{C}$. For each spatial pattern $f$, the mechanism matrices are related to the empirically determined matrix that maps the color of the test input to the observed match by the formula $\mathbf{T}_f = \mathbf{C}^{-1}\mathbf{D}_f\mathbf{C}$. What are the uniqueness properties in our estimate of $\mathbf{C}$ and $\mathbf{D}_f$?

Consider an alternative solution based on a new color matrix $\mathbf{C}' = \mathbf{L}\mathbf{C}$ and a new diagonal pattern matrix $\mathbf{D}_f'$. The new pair of matrices must yield the same $\mathbf{T}_f$. We evaluate the uniqueness of our results by constraining the matrix $\mathbf{L}$.

First, notice that, when $\mathbf{L}$ is a diagonal matrix,

$$\begin{aligned}\mathbf{T}_f = \mathbf{C}^{-1}\mathbf{D}_f\mathbf{C} &= \mathbf{C}'^{-1}\mathbf{D}_f'\mathbf{C}',\\ \mathbf{C}^{-1}\mathbf{D}_f\mathbf{C} &= (\mathbf{L}\mathbf{C})^{-1}\mathbf{D}_f'\mathbf{L}\mathbf{C},\\ \mathbf{C}^{-1}\mathbf{D}_f\mathbf{C} &= \mathbf{C}^{-1}\mathbf{L}^{-1}\mathbf{D}_f'\mathbf{L}\mathbf{C},\\ \mathbf{D}_f &= \mathbf{L}^{-1}\mathbf{D}_f'\mathbf{L},\\ \mathbf{D}_f &\equiv \mathbf{D}_f'.\end{aligned}$$

It follows that any diagonal transformation of $\mathbf{C}$ is permissible and leads to the same diagonal matrix $\mathbf{D}_f$.

Now, consider a proof of the converse, i.e., that only diagonal transformations are permissible. Begin by noting that

$$\mathbf{T}_f = \mathbf{C}^{-1}\mathbf{D}_f\mathbf{C} = \mathbf{C}^{-1}\mathbf{L}^{-1}\mathbf{D}_f\mathbf{L}\mathbf{C},$$

$$\mathbf{D}_f = \mathbf{L}^{-1}\mathbf{D}_f\mathbf{L},$$

$$\mathbf{L}\mathbf{D}_f = \mathbf{D}_f\mathbf{L}. \tag{A1}$$

From inspection of Eq. (A1) we see that the columns of $\mathbf{L}$ are eigenvectors of the diagonal transformation $\mathbf{D}_f'$. The eigenvectors of a diagonal matrix are the unit vectors $(1,0,0)$, $(0,1,0)$ and $(0,0,1)$; thus it follows that $\mathbf{L}$ must be a diagonal matrix.[48]

We state our uniqueness results to show that when we recover a pair of matrices $\mathbf{C}$ and $\mathbf{D}_f$, $\mathbf{LC}$ and $\mathbf{D}_f$ are also solutions only when $\mathbf{L}$ is a diagonal matrix. Hence our estimates of $\mathbf{D}_f$ are unique; our estimates of $\mathbf{C}$ are unique up to three independent scale factors. These scale factors set the overall sensitivity of each appearance mechanism. Intuitively this makes sense; alteration of the scale of any of the three color-tuning functions will preserve the match. We have shown that these scale factors are the only freedom left in the pattern–color-separable solution.

## ACKNOWLEDGMENTS

We thank A. Ahumada, D. Brainard, E. J. Chichilnisky, J. Farrell, and J. A. Movshon. This research was supported by National Eye Institute contract RO1 EY03164, NASA contract 2-307, and an IBM Graduate Student Fellowship.

*Present adress, Center for Neural Science/New York University, Room 809, 4 Washington Place, New York, New York 10003.

## REFERENCES AND NOTES

1. W. K. Pratt, *Digital Image Processing* (Wiley, New York, 1978).
2. M. Rabani and P. Jones, "Digital image compression," Soc. Inf. Displ. Lect. Notes **1,** M-5.1–M5.42 (1990).
3. J. Krauskopf, D. R. Williams, and D. W. Heeley, "Cardinal directions of color space," Vision Res. **22,** 1123–1131 (1982).
4. M. Webster and J. Mollon, "Changes in colour appearance following post-receptoral adaptation," Nature (London) **348,** 235–236 (1990).
5. S. Ishihara, *Tests for Colour-Blindness* (Kanehara Shuppen, Tokyo, 1977).
6. V. Smith and J. Pokorny, "Spectral sensitivity of the foveal cone photopigments between 400 and 500 nm," Vision Res. **15,** 161–171 (1975).
7. R. M. Boynton, *Human Color Vision* (Holt, Rinehart & Winston, New York, 1979).
8. Values in *LMS* color space are given in units of $\mu W/(cm^2\ nm\ sr)$. With use of CIE 1931 XYZ coordinates, the background was $(xyY = 0.27, 0.30, 49.80\ cd/m^2)$.
9. D. H. Brainard, "Calibration of a computer controlled color monitor," Col. Res. Appl. **14,** 23–34 (1989).
10. K. V. Mardia, J. T. Kent, and J. M. Bibby, *Multivariate Analysis* (Academic, New York, 1979).
11. D. H. Brainard and B. A. Wandell, "Asymmetric color matching: how color appearance depends on the illuminant," J. Opt. Soc. Am. A **9,** 1433–1448 (1992).
12. J. P. Chandler, *STEPIT* (Quantum Chemistry Program Exchange, Department of Chemistry, Indiana University, Bloomington, Ind., 1965).
13. The test stimuli from one spatial frequency and one color-direction condition span one dimension in three-dimensional space. We therefore restrict our search for the best-fitting transformation $\mathbf{T}_{f,c}$ to rank-one matrices.
14. B. Efron, *The Jackknife, the Bootstrap and Other Resampling Plans* (Society for Industrial and Applied Mathematics, Philadelphia, Pa., 1982).
15. D. I. A. MacLeod and R. M. Boynton, "Chromaticity diagram showing cone excitation by stimuli of equal luminance," J. Opt. Soc. Am. **69,** 1183–1186 (1979).
16. A. M. Derrington, J. Krauskopf, and P. Lennie, "Chromatic mechanisms in lateral geniculate nucleus of macaque," J. Physiol. **357,** 241–265 (1984).
17. D. I. Flitcroft, "The interactions between chromatic aberration, defocus and stimulus chromaticity: implications for visual physiology and colorimetry," Vision Res. **29,** 349–360 (1989).
18. G. E. Müller, *Darstellung und Erklärung der verschiedenen Typen der Farbenblindheit* (Vandenhoeck-Ruprecht, Göttingen, The Netherlands, 1924).
19. G. E. Müller, "Ueber die Farbenempfindungen," Z. Psychol. **17** and **18** (1930).
20. D. B. Judd, "Response functions for types of vision according to the Müller theory," J. Res. Nat. Bur. Stand. (U.S.) **42,** 1–16 (1949).
21. L. M. Hurvich and D. Jameson, "An opponent-process theory of color vision," Psychol. Rev. **64,** 384–404 (1957).
22. L. M. Hurvich and D. Jameson, "Opponent processes as a model of neural organization, Am. Psychol. **29,** 88–102 (1974).
23. D. Jameson and L. M. Hurvich, "Some quantitative aspects of an opponent-colors theory. I. Chromatic responses and spectral saturation," J. Opt. Soc. Am. **45,** 546–552 (1955).
24. Extensive testing was undertaken to establish the standard, but we have not been able to find the published studies documenting the relationship between color appearance and spatial frequency. We would be grateful for any suggestions.
25. S. L. Guth, "A new vector model," in *Color Metrics,* J. J. Vos, L. F. C. Friele, and P. L. Walraven, eds. (AIC/Holland, Institute for Perception TNO, Soesterberg, The Netherlands, 1972), pp. 82–98.
26. S. L. Guth, "Model for color vision and light adaptation," J. Opt. Soc. Am. A **8,** 976–993 (1991).
27. B. Wandell and D. Marimont, "Axial chromatic aberration and cone-isolation," Invest. Ophthalmol. **33,** 770 (1992).
28. H. H. Hopkins, "The frequency response of a defocused optical system," Proc. R. Soc. London Ser. A **231,** 91–103 (1955).
29. G. Wald and D. R. Griffin, "The change in refractive power of the human eye in dim and bright light," J. Opt. Soc. Am. **37,** 321–336 (1947).
30. R. E. Bedford and G. Wyszecki, "Axial chromatic aberration of the human eye," J. Opt. Soc. Am. **47,** 564–565 (1957).
31. M. A. Georgeson and G. D. Sullivan, "Contrast constancy: deblurring in human vision by spatial frequency channels," J. Physiol. **253,** 627–656 (1975).
32. J. Larimer, D. H. Krantz, and C. M. Cicerone, "Opponent-process additivity—I. Red/green equilibria," Vision Res. **14,** 1127–1140 (1974).
33. J. Larimer, D. H. Krantz, and C. M. Cicerone, "Opponent-process additivity—II. Yellow/blue equilibria and nonlinear models," Vision Res. **15,** 723–731 (1975).
34. C. M. Cicerone, D. H. Krantz, and J. Larimer, "Opponent-process additivity—III. Effect of moderate chromatic adaptation," Vision Res. **15,** 1125–1135 (1975).
35. S. K. Shevell, "The dual role of chromatic backgrounds in color perception," Vision Res. **18,** 1649–1661 (1978).
36. S. K. Shevell and R. A. Humanski, "Color perception under chromatic adaptation: red/green equilibria with adapted short-wavelength-sensitive cones," Vision Res. **28,** 1345–1356 (1988).
37. J. Walraven, "No additive effect of backgrounds in chromatic induction," Vision Res. **19,** 1061–1063 (1979).
38. J. S. Werner and J. Walraven, "Effect of chromatic adaptation on the achromatic locus: the role of contrast, luminance and background color," Vision Res. **22,** 929–944 (1982).
39. O. Schade, "On the quality of color-television images and the perception of colour detail," J. Soc. Motion Pict. Television Eng. **67,** 801–819 (1958).

40. E. M. Granger and J. C. Heurtley, "Visual chromatic modulation transfer function," J. Opt. Soc. Am. **63,** 73–74 (1973).
41. G. J. C. van der Horst and M. A. Bouman, "Spatio-temporal chromaticity discrimination," J. Opt. Soc. Am. **59,** 1482–1488 (1969).
42. C. Noorlander and J. J. Koenderink, "Spatial and temporal discrimination ellipsoids in color space," J. Opt. Soc. Am. **73,** 1533–1543 (1983).
43. A. B. Poirson, B. A. Wandell, D. Varner, and D. H. Brainard, "Surface characterizations of color thresholds," J. Opt. Soc. Am. A **7,** 783–789 (1990).
44. D. H. Kelly, "Spatiotemporal variation of chromatic and achromatic contrast thresholds," J. Opt. Soc. Am. **73,** 742–750 (1983).
45. K. Mullen, "The contrast sensitivity of human colour vision to red–green and blue–yellow chromatic gratings," J. Physiol. **359,** 381–400 (1985).
46. S. Anderson, K. Mullen, and R. Hess, "Human Peripheral spatial resolution for achromatic and chromatic stimuli: limits imposed by optical and retinal factors," J. Physiol. **442,** 47–64 (1991).
47. A. Poirson, "Appearance and detection of colored patterns," Ph.D. dissertation (Stanford University, Stanford, Calif., 1991).
48. We exclude the technical possibility that two entries of $\mathbf{D}_f$ are precisely equal.